

Influences of Rebar Design Parameters on Flexural Properties of Prestressed Beam-column Nodes

Yanpei Cheng¹, Jie Cai² and Ming Chen^{3,*}

¹School of Civil Engineering, Architecture and Environment, Hubei University of Technology, Wuhan 430068, China

²School of Civil Engineering, Architecture and Environment, Hubei University of Technology, Wuhan 430068, China

³School of Automotive and Traffic Engineering, Hubei University of Arts and Science, Xiangyang 441053, China

Received 19 July 2021; Accepted 30 December 2021

Abstract

The beam-column node is an important component of structures and is vital to structural safety. However, existing standards lack design formulas and structural requirements of the Precast Prestressed Efficiently Fabricated Frame (PPEFF) nodes. To investigate mechanical properties of PPEFF nodes deeply, a low-cycle reciprocating load test was conducted on five PPEFF side-node species. Factors such as the failure mode, hysteretic skeleton curve, and ductility of PPEFF nodes were analysed to study their influences on the mechanical properties of the nodes. A previous calculation formula of unbounded prestressed tendon stress growth was modified according to the results of the low-cycle reciprocating load test. Results demonstrate that the hysteretic curves of PPEFF nodes are generally full, and the bearing capacity of the nodes increases significantly with the rise of the reinforcement ratio of unprestressed tendon and initial prestress. However, the energy consumption performance of the nodes declines when the initial prestress is too high. During the modification of the previous calculation formula, it is discovered that when the reduction factor of positive loading (k_1) is 0.28 and the reduction factor of negative loading (k_2) is 0.13, calculation values of the formula agree well with measured values. The obtained conclusions provide a significant reference for the design formula of PPEFF nodes.

Keywords: PPEFF nodes, effective prestress, unprestressed reinforcement ratio, flexural properties

1. Introduction

The beam-column node is an important component of prefabricated concrete structures, and its safety and reliability guarantee the normal services of an entire building. Therefore, beam-column nodes must be adequately strong and rigid, so that energy can be dissipated through the formation and development of plastic hinges during earthquakes. With the increasing contradiction between housing demand and slow construction, convenient and high-efficiency fabricated buildings have been developed accordingly and are becoming popular around the world. Among them, prestressed prefabricated concrete structures feature high construction efficiency, few field wet construction, and light environmental pollution. In recent years, these structures have been widely used in buildings in China. Studies on anti-seismic properties of prestressed prefabricated concrete beam-column nodes are important to ensure these structures maintain good mechanical properties in potential earthquakes.

Compared with traditional cast-in-situ nodes, prestressed prefabricated nodes have diverse forms. According to post-earthquake analysis, the major failures of beam-column nodes occur at the beam-column interfaces. Therefore, Chinese and foreign scholars mainly focus on the connection modes of nodes at beam-column interfaces, such as overall pouring and bolted connection nodes. However, applications of these nodes to practical projects are restricted due to the complex construction process, high cost, and poor

energy dissipation. For example, the core area of overall pouring nodes [1] can easily develop shear cracks and rebar slippage during loading, thereby decreasing the rigidity and energy dissipation performance of the nodes significantly. Although the construction efficiency at the joints of bolted connection nodes [2] is improved significantly, the bolts become damaged to varying degrees after major earthquakes, which causes difficulties for post-earthquake repair, and part manufacturing is too expensive.

Although the beam-column node of Precast Prestressed Efficiently Fabricated Frame (PPEFF) system is modified on the basis of previous studies, this kind of node still lacks reliable experimental data to support its design. Ensuring structural safety, an in-depth study was conducted on the beam-column nodes of PPEFF system.

2. State of the art

The beam-column node is one of the most common and critical connecting nodes in concrete structures. Through long-term studies and practice, several assembly forms have been formed, which generally can be classified into prestressed and unprestressed forms. Compared with unprestressed fabricated nodes, prestressed fabricated nodes are superior due to lower damage and better self-reset performance. Thus, they are highly appreciated by Chinese and foreign scholars. Cooperating with PRESS projects, countries like the United States and Japan have promoted studies on the Hybrid Frame system which is applied to strong earthquake fortification zones, and have carried out

*E-mail address: cm@hbuas.edu.cn

ISSN: 1791-2377 © 2022 School of Science, IHU. All rights reserved.

doi:10.25103/jestr.151.15

low-cycle reciprocating load tests on the system. According to test results, prestressed fabricated nodes have good anti-seismic performance and their energy dissipation performance is as good as cast-in-situ structures. Therefore, prestressed fabricated nodes have been adopted in the design norms of many countries, including the US and New Zealand. Nevertheless, Hybrid Frame system is too complex for construction and has excessively high requirements for in-situ construction quality. Hence, Hybrid Frame system is seldom used in low-level anti-seismic fortification areas because of economic and technological problems. Due to the construction complexity of the Hybrid Frame system, Liang Peixin [3], a Chinese scholar, proposed a new form of post-tensioning unbounded node that eliminates the energy-dissipation rebars that run through the column-beam interfaces below Hybrid Frame. Instead, the energy-dissipation rebars above the beam are connected directly by straight thread sleeves. A low-cycle reciprocating load test was conducted through changing the length of the unbounded section of the energy-dissipation rebars, initial prestressed degree, and reinforcement ratio. According to the test results, damage of the new node mainly concentrates in the beam-column interfaces, and damage of the beams and columns are slight, while its energy-dissipation performance is slightly inferior to the cast-in-situ nodes.

New composites have been applied in the design of beam-column nodes to improve the insufficient bearing capacity of traditional cast-in-situ nodes. Shwan [4] studied reinforced concrete nodes that use new engineering cementitious composite (ECC) and investigated them through a low-cycle reciprocating load test. Moreover, they compared new nodes with ordinary reinforced concrete nodes, and their test mainly focused on crack propagation, hysteretic performance, and energy-dissipation performance. According to the test results, the new ECC-reinforced concrete nodes presented significantly higher anti-shearing and flexural capacities than ordinary reinforced concrete nodes. Due to the high-strength performances of ECC material, the ultimate bearing capacity of new ECC-reinforced concrete nodes is increased to a certain extent, but the energy-dissipation performance is not satisfactory. Shervin [5] discussed the anti-seismic properties of carbon fiber-reinforced plastic (CFRP) reinforced-concrete transverse beam nodes. He constructed six full-size specimens and conducted a reciprocating loading test to study the influence of CFRP on the anti-seismic properties of the nodes. Results demonstrate that the nodes using CFRP reinforcement materials developed small amounts of damage, which could decrease the workloads of post-earthquake node repair. However, CFRP materials are not applicable to temporary large-scale use because of cost concerns. Moreover, CFRP materials are inconvenient for exchange after complete failure of the nodes, which also increases the difficulty of post-earthquake repair. Ali [6] proposed new concrete beam-column nodes filled with fiber-reinforced polymers, and conducted cyclic loading of the nodes by changing the influence of different steel connection lengths on the anti-seismic performance of the nodes. Test results demonstrate that embedding length influences the shear resistance of the nodes. Excessive or insufficient embedding length leads to shortage of flexural properties of the nodes. These need further verification in the future. Khaloodengren et al. [7] analyzed energy dissipation performance, energy dissipation performance, rigidity degradation, and other anti-seismic properties of reinforced

concrete column-steel beam nodes. They found that the assembly of different materials could influence the anti-seismic performance of specimens, which might even be superior to cast-in-situ nodes in terms of performance. Al-Osta [8] replaced concrete in the node region with steel-fiber-reinforced concrete and ultra-high-performance concrete, then conducted monotonous and cyclic loading tests on 10 beam-column nodes. Results demonstrate that concrete nodes in the core region which were replaced by steel-fiber-reinforced concrete and ultra-high-performance concrete presented higher shear resistance and bearing capacity. The failure mode changed from an unsatisfactory shear failure into a bending failure that is more inclined to occur on the beam. These studies mainly concern the influences of new composites on the mechanical properties of the nodes. But they lack theoretical support because the new materials are hardly used in practical engineering. Moreover, the new materials cannot be promoted temporarily at a large scale due to the high cost.

As the joints of beam-column nodes are relatively weak, the connection modes of these nodes are important. Azimi [9] proposed a new connection method of reinforced concrete beam-column nodes, and conducted numerical simulation and static cyclic loading experimental studies by using "anti-torque spirals". In these experimental studies, ordinary rectangular spiral columns were compared with columns in the conventional reinforcement system; results show that the nodes connected in the new way have better ultimate lateral resistance, ductility, and energy-dissipation performance. Nzabonimpa [10] proposed a type of dry mechanical beam-column node for fully constrained bending moment connectors of concrete components. These new nodes are composed of ductile steel plates with bolts to transmit tensile force and pressure and provide fully constrained torque connections at beam-column joints. Besides, a cyclic loading test was carried out on six new specimens. Results show that after reaching the maximum loads, the loads decline quickly without evident deformation. The major deformation is near the beam-plate joint, and the overall energy dissipation performance of the specimens was relatively poor. Vidjeapriya et al. [11] and Naik et al. [12] proposed a prefabricated concrete beam-column node with brackets and a splint angle. The prefabricated components were connected by rebars or steel plates through overlapping, welding or bolts, and a reverse cyclic loading test was conducted. According to test results, shear resistance of the structure is improved because of the prestress effect and the specimens have good recovery capability after unloading. Aydin [13] only performed loading on tests of eight specimens for bolted connection of beam-column nodes with and without stiffening ribs. Results demonstrated that specimens with stiffening ribs have higher flexural performance and rigidity, but the overall ductility is relatively lower. Girgin [14] conducted a low-cycle reciprocating load test on one overall framework and five prefabricated hybrid semi-proportional nodes by changing the longitudinal welding coefficient. Results show that the bending rebars at the beam bottom play an important role in the general mechanical properties of nodes and the failure modes of the nodes vary significantly with the welding coefficients.

To increase the energy-dissipation capacity of prefabricated prestressed nodes, some scholars tried to install various devices at the beam-column connections. For example, Morgen et al. [15-17] installed the frictional energy-dissipation damper at no-sticking points to improve

the energy dissipation performance of prestressed nodes; the test results demonstrated that the energy-dissipating capacity was strengthened by adding the friction damper. Moreover, the nodes recovered well after unloading because of prestress, and the residual deformation was small. However, the damper incurred a high manufacturing cost and was applicable to only a few node types. Thus, it has not been widely used on a temporary basis.

Considering the cost of new materials and uncertainty of properties, some Chinese scholars focus on the reconstruction of prestressed prefabricated beam-column nodes based on traditional cast-in-situ nodes. For example, Zhang Chen et al. [18] carried out a pseudo-static test on Post-tension Unbonded Hybrid Prefabricated (PTHP) nodes and found that PTHP nodes have good energy dissipation performance, strong ultimate-bearing capacity and slight residual deformation after unloading. Pan Peng et al. [19] carried out a low-cycle reciprocating load test on PPEFF nodes and compared PPEFF nodes with cast-in-situ nodes. According to the test results, PPEFF nodes have the same excellent anti-seismic performance as the hybrid frame nodes. Given adequate construction efficiency and material cost, PPEFF nodes have good ductility and restoration performance. Except for slightly lower energy dissipation performance, these nodes are superior to cast-in-situ nodes in bending and shear resistance and have enough safety reserves.

Based on previous studies and existing limitations, the beam-column nodes of the PPEFF system were reconstructed in this study. Two web reinforcements were added on the interface of PPEFF system to improve the shear resistance of the nodes, prevent collapse of overall structures due to sudden failures of prestressed rebars, and to improve the safety of overall structures. The plastic hinge region at the beam ends was consolidated to strengthen the plastic hinge region of the node zone. The node beams used overlapping components and were divided into prefabrication and cast-in-situ layer. A 200 mm thick post-pouring layer was left at the upper parts of the beam, which was convenient for installation of the energy-dissipation and shear rebars and increased the construction efficiency. In this experiment, five PPEFF beam-column side nodes were selected for the low-cycle reciprocating load test to analyze their failure characteristics and flexural properties as well as further optimize the ranges of the rebar design parameters of PPEFF nodes. Meanwhile, the formula of increments of the unbonded prestressed tendons, which was corrected by test data, was verified, providing theoretical support for the design of PPEFF nodes.

The rest of this study is organized as follows. Section 3 introduces the low-cycle reciprocating load test. Section 4 analyzes the test results of the failure mode, bearing capacity, and hysteretic behaviors of PPEFF nodes, and discusses the influences of relevant rebar design parameters on the mechanical properties of the nodes. Meanwhile, the reliability of the optimized formula is verified by the test data. Section 5 summarizes the conclusions.

3. Methodology

3.1 Structural characteristics of the nodes

For convenience of transportation and installation, both beams and columns used regular prismoids. The prefabricated beam was a superposed component. A 200 mm thick post-pouring layer was left, which increased the

convenience of rebar installation and improved the field construction efficiency. In PPEFF nodes, the ordinary energy-dissipation rebars and shear rebars that run through the beam-column interfaces were only set at the upper surfaces of the beam. A 300 mm length unbonded section was set on the energy-dissipation rebars at the upper part of the prefabricated beams to avoid early yielding of rebars due to concentrated stress in the loading process. The shear rebars were set at the beam ends to prevent the nodes from losing bearing capacity upon accidental breakage of the prestressed tendons, thereby improving the safety of the structure. A 200 mm thick post-pouring layer was left at the upper part of the prefabricated beam for convenient energy dissipation and installation of the shear rebars. The prestressed tendons were free of bonding throughout the length and they penetrated the preserved pore channels of the beams and columns. The fixed end was at the beam end and the jacking end was the column end. No grouting was provided after finishing stretching-drawing. A 20 mm high-strength fissure of cementation on the beam-column interfaces was left. Stirrups in the plastic hinge region of the beam end were densified to increase the strength of the plastic hinge region of the nodes. The manufacturing process of nodes is shown in Fig. 1.

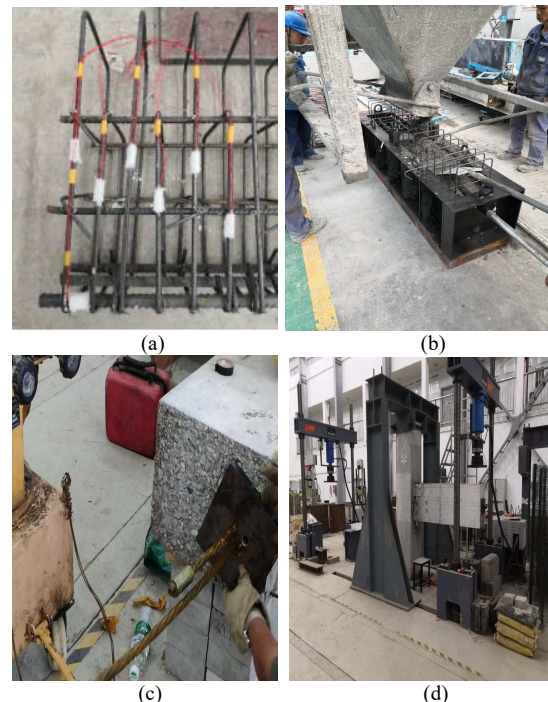


Fig. 1. Test piece production process. (a) Strain gauge binding. (b) First casting in situ. (c) Tensile prestressed tendons. (d) Specimens in position

3.2 Specimen design

In this test, 5 PPEFF node specimens were named JD1, JD2, JD3, JD4, and JD5. Design parameters of the specimens are shown in Table 1 and reinforcement conditions are shown in Fig. 2. Layout of the experimental apparatus is shown in Fig. 3. The test focuses on the influences of the initial effective prestress of the unbonded prestressed tendons and reinforcement ratio of the non-prestressed tendons on the flexural properties of the nodes. Bearing capacity, ductility, strain laws of unprestressed rebars, and stress increment of the unbonded prestressed tendons of the specimens were analyzed. All the beams and columns of the specimens were made of C40 concrete. The cube crushing strength and elasticity modulus of concrete were measured at 42.6 Mpa

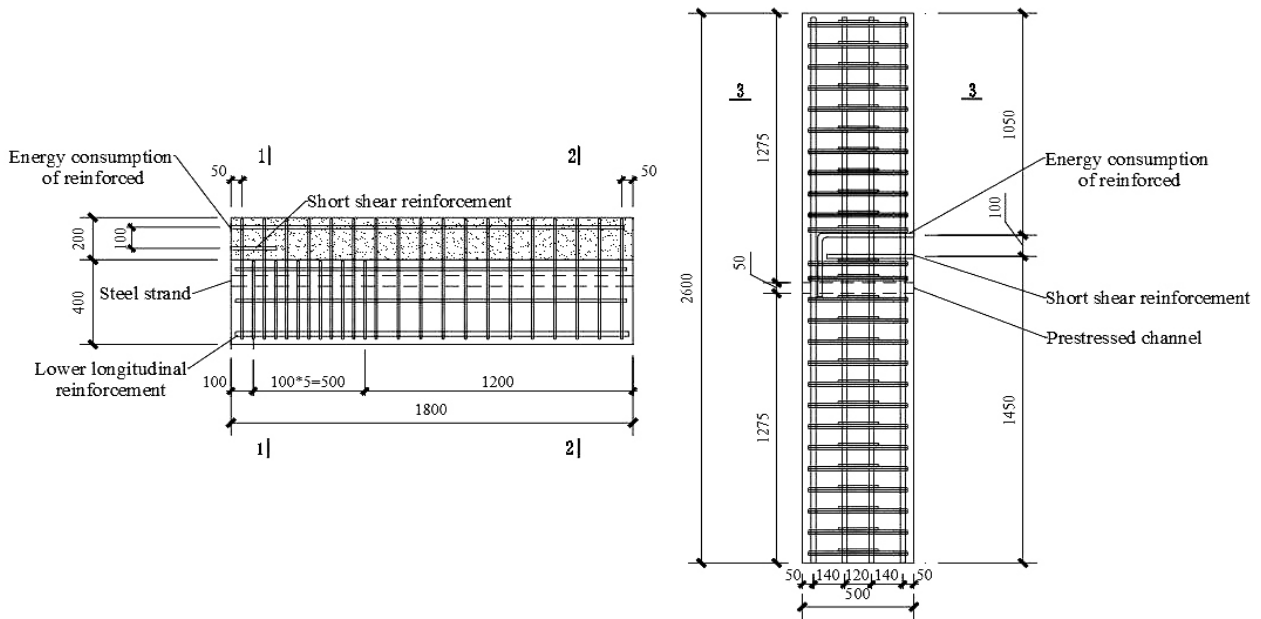
and 3.31×10^4 Mpa respectively. Longitudinal bars, stirrups, and structural rebars of the beams and columns were all HRB400-level rebars. The prestressed tendons composed of three pieces of steel strands with a diameter of 15.2 mm. The tensile strength was 1860 Mpa and the rebar material properties are listed in Table 2.

Table 1. Specimen design parameters

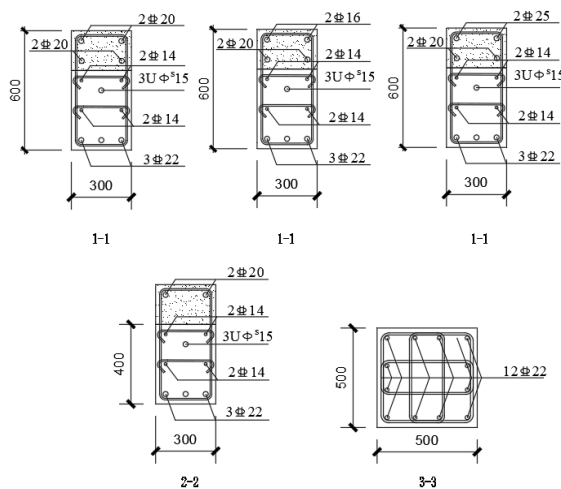
Specimen number	Initial prestress of steel strand(Mpa)	Non-prestressed reinforcement ratio(%)
JD1	950	1.45
JD2	1150	1.45
JD3	1350	1.45
JD4	1150	1.32
JD5	1150	1.67

Table 2. Reinforcing steel material properties

Steel types	Steel grade	Steel bar diameter (mm)	Yield strength (Mpa)	Ultimate strength (Mpa)	Modulus of elasticity
Prestressed reinforcement	Steel strand	15.24	1823	1981	1.96×10^5
Ordinary reinforced	HRB400	16	489.83	632.24	1.99×10^5
	HRB400	20	549.27	786.13	2.01×10^5
	HRB400	25	686.59	982.67	2×10^5



(a)



(b)

Fig. 2. Specimen reinforcement. (a) Structure of nodes. (b) Column-beam section details

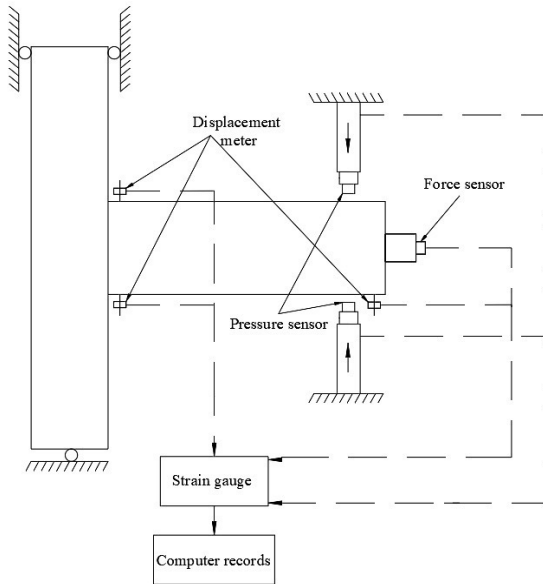


Fig.3. Arrangement of test instruments

3.3 Experimental apparatus and loading schemes

In this experiment, specimens were transported by cranes and nodes were fixed on the ground through a ground anchor. The ratio between the axial pressure which was exerted to the column top by the oil jack and the axial pressure at prestressed top was 0.2. The column end and top were tight but allowed free rotation, thus enabling the transmission of counterforce from the column end to the counter frame. A rubber bearing was placed at the column top to simulate the hinge support of the column end. The loading device was WHY-500 microprocessor control compression testing device and the acquisition device was Donghua DH3816N static data acquisition instrument. It was set that the downward loading was positive and upward loading was negative. Loading was divided into load control stage and displacement control stage. Load control was applied before yielding of the nodes. Loads of P_1 , P_2 , and P_3 ($P_1 = 30.5\text{kN}$, $P_2 = 42.7\text{kN}$, $P_3 = 61\text{kN}$) were adopted for the gradual loading at the beam end of the nodes and each level of loading circulated once. When the nodes entered the yielding state, displacement control started. Let the displacement of the beam end be Δ and $n\Delta$ ($n=1, 2, 3, 4, \dots$) was adopted for gradual loading. Each level of displacement loading circulated twice. When the loads were lower than 85% of the ultimate loads, the bearing capacity of the specimens decreased. The specimens failed and the loading terminated. The loading program of the specimens is shown in Fig. 4.

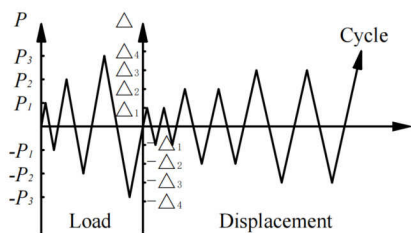


Fig.4. Loading System

4. Result Analysis and Discussion

4.1 Failure modes of specimens

The failure mode of JD1 is shown in Fig. 5(a). In the force control stage, the beam section began to crack and the crack with a width of approximately 0.15 mm when the negative loads reached 30.52 kN. In the displacement control stage (1–2 Δ), numerous vertical cracks and inclined cracks occurred on the concrete in the unbonded section of the energy-dissipation rebars and the crack width was approximately 2.5 mm. The maximum width of the vertical crack on the beam-column interface was 10 mm and a transverse crack occurred at the lower part of the back of the column core region, which was approximately 0.05 mm wide. In the displacement stage (3–4 Δ), the transverse crack extended into a run-through crack which was approximately 0.1 mm wide. Meanwhile, concrete at the beam-column bottom began to fall off and numerous cracks occurred on the concrete in the range of about 400 mm from the beam top to the beam-column interface. Concrete at two sides in a range of approximately 100 mm to the beam-column interface were crushed and fell off, exposing the energy-dissipation and shear rebars. The failure mode of JD2 is shown in Fig. 5(b). In the force control stage, the negative loads reached 42.75 kN and cracks began to develop on the upper part of the prefabricated beam, which were approximately 0.1 mm wide. In the displacement control stage (1–2 Δ), many inclined cracks occurred in a range of 400 mm near the beam-column interface, which were approximately 2 mm wide. Transverse run-through cracks were developed on the concrete on top of the prefabricated beam, which were about 8 mm wide. In the displacement control stage (3–4 Δ), the concrete on top at about 300 mm near the beam-column interface were crushed and fell off, exposing the energy-dissipation and shear rebars. The energy-dissipation rebars formed heaves in the unbonded section. The failure mode of JD3 is shown in Fig. 5(c). In the force control stage, cracks began to develop when negative loads reached 61.21 kN, which were approximately 0.05 mm wide. In the displacement control stage (1–2 Δ), a great number of inclined cracks were developed on concretes at the upper part of the beams and several transverse run-through cracks occurred at the top of the beams, which were about 0.15 mm wide. Numerous small micro-vertical cracks and inclined cracks developed on the concrete at the upper parts of the beams within 300 mm to the beam-column interface, which were about 0.2 mm wide. Two transverse cracks were developed at the lower part of the back of column core zone, which were about 0.05 mm wide. In the displacement control stage (3–4 Δ), lots of concrete failures were detected at the upper part of beams approximately 350 mm to the beam-column interface were detected, exposing the energy dissipation and shear rebars. Moreover, many inclined cracks were observed on the concrete at the upper part of the beams. The failure mode of JD4 is shown in Fig. 5(d). In the force control stage, cracks that were about 0.1 mm wide began to develop when negative loads reached 29.65 kN. In the displacement control stage (1–2 Δ), many inclined cracks developed on the concrete at the beam-column interface, which were approximately 2.5 mm wide at most. The largest crack on the beam-column interface was approximately 8 mm. In the displacement control stage (3–4 Δ), the concrete in a triangle region at the upper part of the beam fell off. Concrete damage was serious in a range of up to that was 0–400 mm away from the beam-column interface. The failure mode of JD5 is shown in Fig. 5 (e). In the force control stage, cracks that were about 0.1 mm wide began to develop on the concrete at the beam sides when loads reached 42.5 kN. In the displacement control stage (1–2 Δ),

the concrete on the beam-column interface were crushed slightly. Concrete cracks at the upper part of the beam were approximately 1.5 mm wide at most, while the maximum crack width at the beam-column interface was 7mm. In the displacement control stage (3–4Δ), concrete at the upper part of the beam-column interface was damaged at a large scale and heaved up. Moreover, the energy-dissipation rebars heaved up and transverse cracks at about 0.5 mm wide developed on the back of the column core zone. Concrete at the unbonded section of the energy-dissipation rebar fell off, thereby exposing the energy-dissipation and shear rebars.

According to the failure modes of the five specimens, with the increase of the initial effective prestress of the prestressed tendons and reinforcement ratio of the unprestressed tendons, the crack width decreases but the crack distribution intensity increases gradually. The prestressed tendons restrict the production and expansion of cracks effectively. The involvement of the unprestressed tendons delays the action of the prestressed tendons. During the loading, PPEFF nodes do not develop shear slip, indicating that the shear reinforcement on the upper part of the beam and friction of the beam-column interface could meet the requirements of shear resistance completely. After unloading, the beam-column interfaces of the five specimens basically closed and the failures were relatively concentrated, accompanied with slight residual deformation.

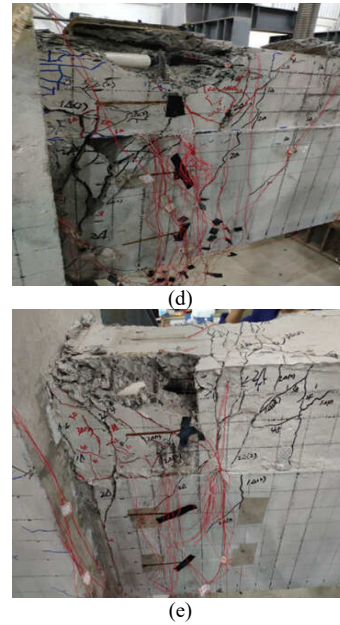
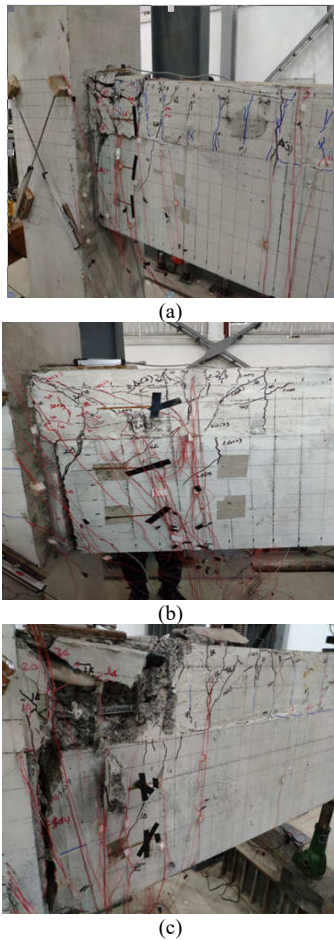
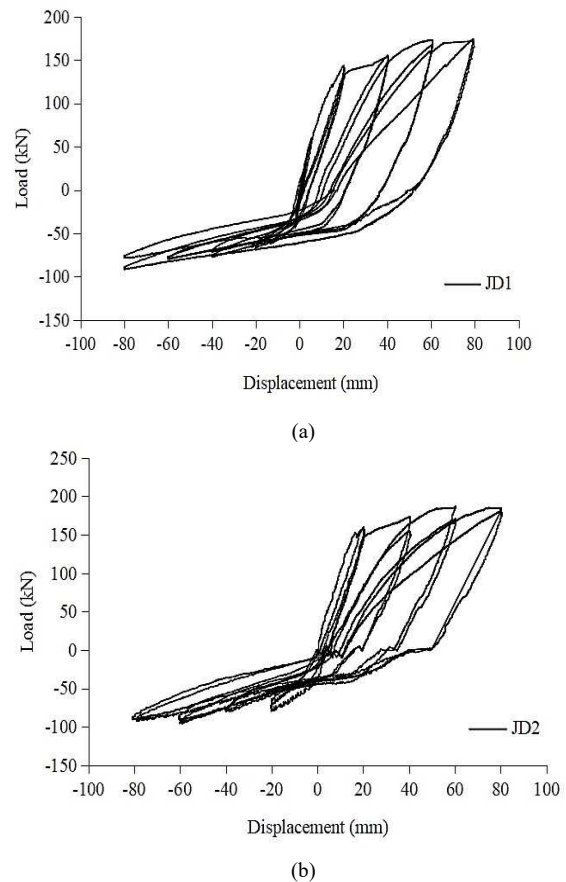


Fig.5. Specimen damage. (a) Failure of JD1. (b) Failure of JD2. (c) Failure of JD3. (d) Failure of JD4. (e) Failure of JD5

4.2 Bearing capacity analysis of specimens

The load-displacement curves of the beam ends of JD1, JD2, JD3, JD4 and JD5 are shown in Fig. 6.



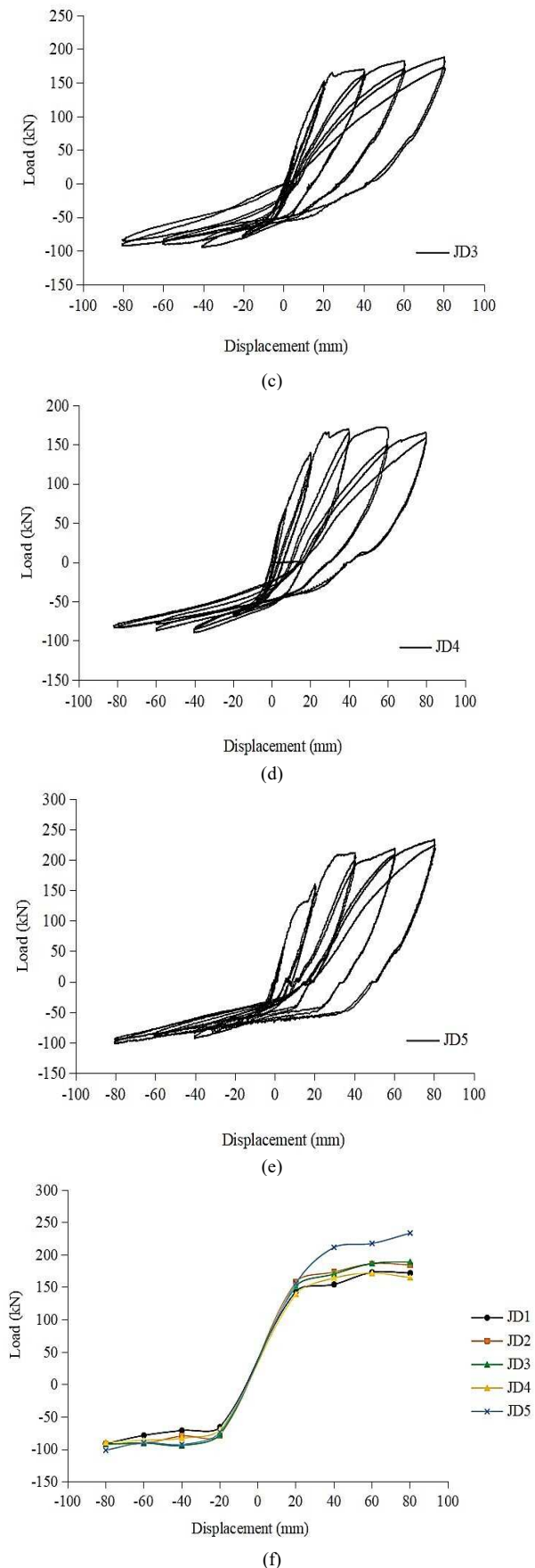


Fig.6. Specimen hysteresis skeleton curve. (a) JD1 hysteresis curve. (b) JD2 hysteresis curve. (c) JD3 hysteresis curve. (d) JD4 hysteresis curve. (e) JD5 hysteresis curve. (f) Specimen skeleton curve

Fig.6 indicates that:

(1) Residual deformation of the five specimens after unloading is relatively slight and the hysteretic curves linger around the original point. Since the rebars were arranged asymmetrically on the beam-column interfaces, the curves are relatively flat and the hysteretic curves are full during positive loading (negative bending moment), indicating good energy dissipation performance. During negative loading (positive bending moment), the curves are relatively steep, and the hysteretic curves are flat, indicating poor energy dissipation performance. With the increase of the initial effective prestress of the prestressed tendons, the “shrinking” of curves become more obvious. This result reflects that higher initial effective prestress of the prestressed tendons leads to stronger restoration capacity of the nodes, and the ultimate loads of the specimens increase to a certain extent with the increase of the displacement at the beam ends. With the increase of the reinforcement ratio of the unprestressed tendons, the hysteretic curves of the specimens tend to be full and the energy dissipation performance increases accordingly. As a result, positive and negative ultimate bearing capacities of the specimens are improved significantly. This proves that instead of the effective prestress, the unprestressed tendons is the major factor that influences the ultimate bearing capacity of the specimens. In general, the hysteretic curves of the five specimens present shrinkage to different degrees and the residual deformations of the nodes are relatively slight due to the existence of prestressed tendons.

(2) According to a comparison of the different cycles of displacement at the same level, the hysteretic curve of the last loading has a similar slope as that of the previous loading. This result demonstrates that when influenced by prestress, specimens have good restoration capacity, while rigidity and strength degrade slightly. During various displacements of the same specimen, the slope of the curve decreases gradually, which shows that the rigidity of the specimens degrades in response to reciprocating loads.

(3) With the increase of loading displacement, energy dissipation of the nodes increases gradually, indicating continuous strengthening of energy dissipation performance. However, the shrinkage of the hysteretic ring of JD3 is more obvious than that of JD1. This means excessive prestress may decrease the energy dissipation performance of the specimens. The main reason is that the clamp force of the beam-column interface increases when the prestress increases, which also inhibits deformation of the specimens and decreases their energy dissipation performance. The hysteretic ring of JD5 is fuller than those of JD2 and JD4. In the value range of the reinforcement ratio of the unprestressed tendons, a higher unprestressed reinforcement ratio indicates better energy dissipation performance of the specimens.

(4) The skeleton curves of the five specimens are basically consistent. All specimens experience elasticity, yielding, strengthening, ultimate, and failure stages during the reciprocating loading process. The positive ultimate bearing capacity of JD3 is 8.41% higher than that of JD1, and the negative ultimate bearing capacity of JD3 is 1.86% higher than JD1. In the value range of prestress in this experiment, higher initial effective prestress exerted by the prestressed tendons leads to higher ultimate bearing capacity of the specimens. The positive ultimate bearing capacity of JD5 is 20.12% higher than JD4 and the negative ultimate bearing capacity of JD5 is 8.36% higher than that of JD4. In the value range of the reinforcement ratio of the unprestressed tendons in this experiment, the ultimate

bearing capacity of the specimens is positively related with the reinforcement ratio of the unprestressed tendons. The reinforcement ratio of the unprestressed tendons could improve the ultimate bearing capacity of the nodes more than the initial effective prestress.

4.3 Ductility analysis of the specimens

The ductility of the structure is typically expressed by a ductility factor. Ductility is the ability of a section of a structure or component to deform from the onset of yielding to the maximum load-carrying capacity or beyond without a

significant drop in load-bearing capacity. In anti-seismic design, ductility is an important index that is usually expressed by the ductility coefficient (μ): $\mu = \Delta_y / \Delta_u$, where Δ_y is the displacement of the characteristic point under the ultimate state and Δ_u is the displacement of the characteristic point under the yield state. The ductility coefficients calculated during positive and negative loading of JD1–JD5 are shown in Table 3.

Table 3. Specimen displacement ductility

Specimen number	Loading direction	Yield displacement Δ_u (mm)	Limit displacement Δ_y (mm)	Displacement ductility coefficient
JD1	Positive	21.2	80.06	3.78
	Negative	3.76	79.78	21.22
JD2	Positive	21.03	80.11	3.81
	Negative	3.14	79.59	25.35
JD3	Positive	20.91	80.04	3.83
	Negative	2.92	79.32	27.16
JD4	Positive	20.60	80.16	3.89
	Negative	2.92	79.21	27.13
JD5	Positive	21.65	80.52	3.72
	Negative	4.31	79.65	18.46

Table 3 shows that the ductility coefficients of the five specimens under positive and negative loadings differ significantly. When JD1, JD2, and JD3 undergo positive loading, the ductility coefficients of the nodes are in the range of 3.78–3.83, which is close to that of ordinary reinforced concrete nodes. When specimens undergo negative loading, the ductility coefficients of the nodes are in the range of 21.22–27.16. JD3 has the highest ductility, followed by JD2 and JD1 successively. Clearly, the ductility of the nodes is negatively related to the initial effective prestress of the specimens. When JD4, JD2 and JD5 undergo positive loading, the ductility coefficients of the nodes are in the 3.72–3.89 range. When the specimens undergo negative loading, the ductility coefficients of the nodes are in the range of 18.46–27.13. JD4 has the highest ductility, followed by JD2 and JD5 successively. This result proves that the ductility of nodes is negatively related to the reinforcement ratio of the unprestressed tendons. To sum up, the energy-dissipation rebars and prestressed tendons bear tensile stress together under positive loading and the beam-end displacement is relatively great when the nodes reach the ultimate state. When the nodes undergo negative loading, the prestressed tendons bear the tensile effect, and the beam-end displacement when the nodes reach the ultimate state is relatively small. Thus, the ductility coefficients of the nodes under negative loading are far higher than those of the nodes under positive loading. Besides, the unprestressed reinforcement ratio influences the ductility of the specimens more than the initial effective prestress.

4.4 Strain laws of the unprestressed tendons

Based on the experiment, the “plastic hinge” of the beam end breaks down at the failure of the PPEFF nodes. The rebar deformation of the beam end generates plastic strains with the development of the beam-end plastic hinges and promotes the energy dissipation performance of the specimens in the late loading stage. Due to the constraints of the prestressed tendons, the plastic deformation of the core zone of the nodes is restricted and the initial rigidity of the nodes increased, thereby prolonging the time for nodes to reach yielding. The effect of the prestressed tendons can be

manifested by the strain of the energy-dissipation rebars at the upper part of the beams. Considering the failure of the strain gangle in the displacement control loading stage, the displacement control stage (1Δ) is chosen and the energy-dissipation rebar strain laws are shown in Fig. 7.

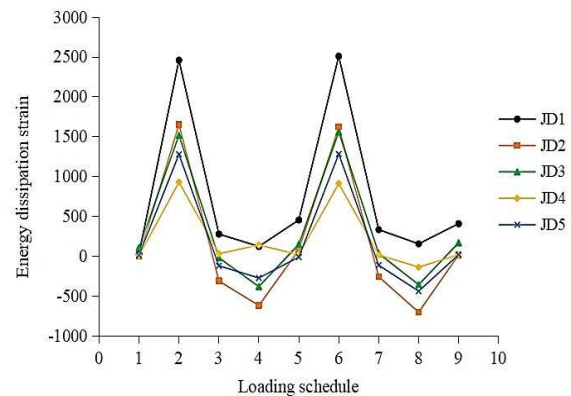


Fig.7. Energy-consuming steel strain law

Fig. 7 shows that under low-cycle reciprocating loads, the strain laws of the energy-dissipation rebars are relatively uniform and the curves generally present basically the same variation trend. For PPEFF nodes, the stress conditions of the rebars decrease effectively because of the existence of the prestressed tendons. In the prestress value range of this experiment, rebars take a longer time to yield when the initial effective prestress of the prestressed tendons is higher, thereby improving the anti-seismic performance of the prefabricated components. By contrast, the influences of the reinforcement ratio of the unprestressed tendons on the strain laws of rebars are not obvious.

4.5 Influence analysis of the stress increment of the prestressed tendons

In the unbonded prestressed concrete nodes, the influencing factors of flexural properties include the reinforcement ratio of the unbonded prestressed tendons, comprehensive reinforcement indexes, concrete strength level, and initial

effective prestress of the prestressed tendons. In this section, the focus is on the influence of the initial effective prestress of the prestressed tendons and the reinforcement ratio of the unprestressed tendons on the stress increment of the prestressed tendons.

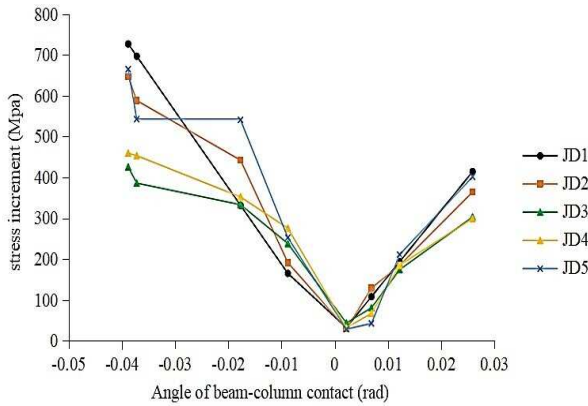


Fig.8. Prestressing tendon stress increment

The stress increment corner relations of the five specimens were tested. (Fig. 8)

(1) With the increase of the intersection angle of the beam-column interface of the PPEFF nodes, the deformation of the prestressed tendons increases and so does the stress increment. The prestressed tendons are always in the elastic working state and provide a bending moment of self-restoration for the prefabricated nodes. Although the beam-column interface opens and closes continuously when the PPEFF nodes are under the low-cycle reciprocating load test, they realize self-restoration after each unloading. However, the nodes also develop plastic deformations that lead to a certain loss of prestress. Moreover, prestress loss increases with the increase of the beam-end displacement.

(2) Mechanical behaviors of the beam-column interface under positive and negative loadings are significantly different because of different asymmetric arrangements of the rebars. Under positive loading (negative bending moment), the energy-dissipation rebars, shear rebars, and unbonded prestressed tendons bear the pressure together. Therefore, the stress increment produced by the prestressed tendons is relatively small. Under negative loading (positive bending moment), only the prestressed tendons and shear rebar assume the tensile loads. Thus, the stress increment produced by the prestressed tendons is relatively high during negative loading.

(3) Under positive loading, the stress increment of the prestressed tendons differs slightly, indicating that the energy-dissipation rebars bear a part of the bending moment. During negative loading, the rank of the specimens' increments is as follows: JD1>JD5>JD2>JD4>JD3. These results reflect that the smaller the initial effective prestress is, the later the tendons participate in the tensile effect. As the energy-dissipation rebars assume compression during negative loading, the stress increment of the prestressed tendons is positively related to the unprestressed reinforcement ratio.

4.6 Stress increment calculation of the prestressed tendons

4.6.1 Stress state analysis of the prestressed tendons

The calculation of the ultimate stress increment of the prestressed tendons is the key in calculating the stress design value of the unbonded prestressed tendons. Based on analysis of the experiment, the initial effective prestress of the prestressed tendons and the reinforcement ratio of the unprestressed tendons significantly influence the ultimate stress increment of the unbonded prestressed tendons.

The following basic hypotheses were applied in the deduction process:

(1) Friction between the unbonded prestressed tendons and the preserved pore channel wall is ignored.

(2) The unbonded prestressed tendons are viewed as the ideal linear elastic material.

(3) The energy-dissipation rebars reach the yielding state under ultimate state and the unbonded prestressed tendons maintain elasticity all the time. The concrete failure mode is crushing failure.

The energy-dissipation rebars, shear rebars, and prestressed tendons running through sections are set on the beam-column interface. Under low-cycle reciprocating loading, ordinary rebars yield and deform under repeated tension and compression, thereby realizing the goal of dissipating seismic energies. Moreover, the energy-dissipating rebars, shear rebars, and prestressed tendons connect beams and columns together by running through the beam-column interface and provide bending capacities for the nodes. The mechanical characteristics of the section under the ultimate stress state of the concrete are shown in Fig. 9.

In Fig. 9, δ_p is the deformation volume of the unbonded prestressed tendons; δ_i is the corner of the beam-column interface; T_e is the resultant force produced by the energy-dissipation rebars on the interface; T_s is the resultant force produced by the shear rebar on the interface; T_p is the resultant force produced by the interface; T_e' is the resultant force produced by longitudinal bars at the beam bottom on the interface; C_c is the resultant force produced by concrete in the compression zone; x_a is the height of the concrete compression zone. When unbonded prestressed tendons reach the proportional limit, the corner of beam-column interface is calculated as follows:

$$\theta_i = \varphi_y L_{pu} \tag{1}$$

The yield curvature of the section is

$$\varphi_y = \frac{\varepsilon_{cy}}{(0.5h - x_a)} = \frac{f_{py} - \sigma_{pe}}{(0.5h - x_a)E_p} \tag{2}$$

The ultimate stress increment of the prestressed tendons is

$$\Delta\sigma_p = E_p \Delta\varepsilon_p = \frac{E_p (0.5h - x_a) \theta_i}{L_{pu}} \tag{3}$$

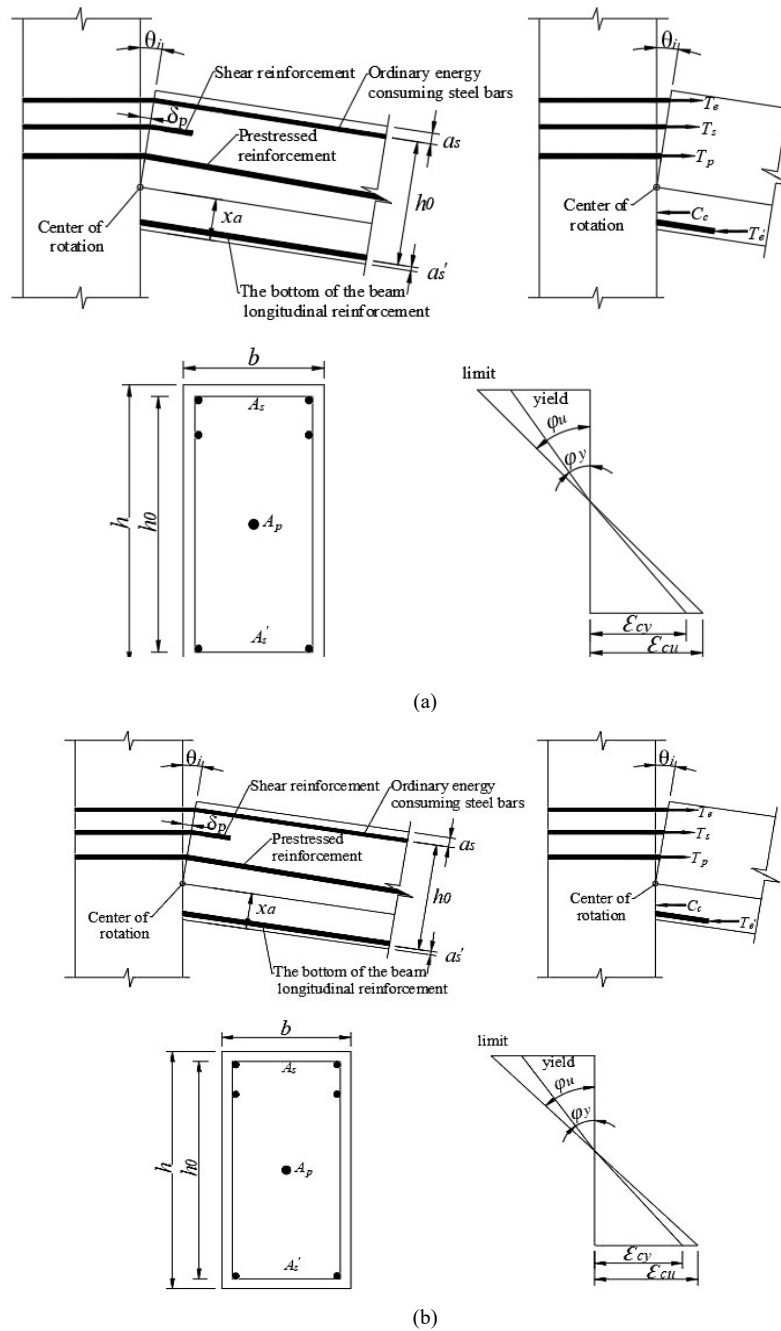


Fig.9. Balance of internal forces on the section in yield limit stage. (a) Balance relations of the internal forces on the section in yield limit stage of the nodes under positive loading (b) Balance relations of the internal forces on the section in yield limit stage of the nodes under negative loading

The height of the concrete equivalent rectangular compression zone (x_a) is estimated theoretically and the height coefficient k of the compression zone is introduced. They are calculated as follows:

$$k = \sqrt{(\rho + \rho')^2 n^2 + 2\left(\rho + \frac{\rho' a_s'}{h_0}\right)n} - (\rho + \rho')n \quad (4)$$

The height of the neutral axis (x_c) is

$$x_c = kh_0 \quad (5)$$

Then, the height of the concrete equivalent rectangular compression zone (x_a) is

$$x_a = 0.8x_c \quad (6)$$

In Eq. (1)~(6):

φ_y is the yielding curvature of section; f_{py} is the proportional limit of unbonded prestressed tendons; L_{pu} is the anchoring length of unbonded prestressed tendons; ρ is the reinforcement ratio of tensile rebars, $\rho = A_s / bh_0$; ρ' is the reinforcement ratio of compression rebars, $\rho' = A_s' / bh_0$; n is the ratio of elasticity modulus of rebars and concrete.

4.6.2 Ultimate stress increment formula of prestressed tendons

Based on test results and the preceding analysis, major factors that influence the stress increment of the prestressed

tendons include the calculation length of the bending component, initial effective prestress, and reinforcement ratio of the unprestressed tendons. As the initial effective prestress increases, the stress increment rises. As the reinforcement ratio of the prestressed tendons increases, the stress increment declines. As the reinforcement ratio of the unprestressed tendons increases, the stress increment also increases.

As the mechanical behaviors of the beam-column interface vary under positive and negative bending moments, the energy dissipation rebars, shear rebars, and the prestressed tendons bear the bending moment together under the negative bending moment. Under the positive bending moment, only the shear rebars and prestressed tendons bear the bending moment together. Due to the shrinkage and creeping of the concrete and the retraction of the anchoring tools, stress losses are produced by friction between the prestressed tendons and the preserved pore channels during the loading. With reference to the content in article 10.1.14 in the Design Norms of Concrete Structure [20] and the formula of the unbonded prestress increment proposed by previous researchers [21], a calculation formula of prestress increment that is applicable to PPEFF nodes is proposed. For convenience in practical engineering applications, the formula ignores some secondary influencing factors and the ultimate stress increment produced by prestressed tendons is calculated according to the following equations:

$$\Delta\sigma_p = 110 + \frac{10f_c(1-\rho)}{k_1\sigma_{pe}\rho_p} \tag{7}$$

$$\Delta\sigma_p = 110 + \frac{10f_c(1-\rho)}{k_2\sigma_{pe}\rho_p} \tag{8}$$

In Eq. (7)–(8),

σ_{pe} is the initial effective prestress of unbonded prestressed tendons; f_c is the design value of axial compressive strength of concrete; ρ_p is the reinforcement ratio of unbonded prestressed tendons; ρ is the reinforcement ratio of unprestressed tendons; k_1 is the reduction factor under positive loading, $k_1 = 0.28$; k_2 is the reduction factor under negative loading, $k_2 = 0.13$.

Increment values of ultimate stress of the prestressed tendons are calculated from Eqs. (7) and (8) and compared with measured values. Comparisons in Table 4 show high agreement, which proves that the theoretical formula is reliable to a certain extent.

Table 4. Comparison between formula calculated value and measured value

Specimen number	Loading direction	$\Delta\sigma_{p1}$ (MPa)	$\Delta\sigma_{p2}$ (MPa)	$\Delta\sigma_{p1} / \Delta\sigma_{p2}$
JD1	Positive	397.22	415.60	0.96
	Negative	728.62	728.21	1.00
JD2	Positive	347.27	365.67	0.95
	Negative	621.04	647.71	0.96
JD3	Positive	312.12	304.45	1.03
	Negative	545.33	426.82	1.28
JD4	Positive	347.27	297.00	1.17
	Negative	614.29	460.84	1.33
JD5	Positive	343.30	402.83	0.85
	Negative	612.50	666.35	0.92

Note: $\Delta\sigma_{p1}$ is the calculated value of the ultimate stress increment of an unbonded prestressed tendon, while $\Delta\sigma_{p2}$ is the measured value.

5. Conclusions

To explore the mechanical properties of PPEFF nodes deeply and provide calculation references and tectonic requirements related to PPEFF nodes, this study conducted low-cycle reciprocating load tests of five PPEFF nodes with different parameters. Meanwhile, mechanical properties of specimens, including failure modes, hysteresis skeleton curves, displacement ductility, and strain laws of energy-dissipation rebars were analyzed. Finally, existing formulas were corrected by measured data.

The following main conclusions can be drawn:

(1) Failure behaviors of PPEFF nodes mainly concentrate near the beam-column interface, which are mainly manifested as one principal crack on the beam-column interface and local crushing of the concrete on the beam surface. Concrete failure in the upper part of the beams is serious, whereas damage in the core zone and prefabricated column is mild. This condition can meet design requirements of “strong column and weak beam”. During the loading process, unbonded prestressed tendons always maintain elasticity and the nodes have good deformation restoration. Due to the asymmetric layout of rebars on the beam-column interface, hysteretic curves are full under positive loading (negative bending moment), and the energy dissipation is

good. Under negative loading (positive bending moment), hysteretic curves are shriveled, and the energy dissipation is poor.

(2) Increasing the initial effective prestress of prestress tendons and the reinforcement ratio of unprestressed tendons can increase the ultimate bearing capacity of specimens. Under positive loading, the energy-dissipation rebars and prestressed tendons mainly assume the tensile effect. Specifically, energy-dissipation rebars assume the highest tensile effect. Under negative loading, prestressed tendons assume the tensile effect, while concrete and energy-dissipation rebars assume the compression effect. In the value range of this test, given the same initial prestress, the bearing capacity of specimens is higher when the unprestressed reinforcement ratio is 1.67%. Given the same unprestressed tendons, the bearing capacity of specimens is higher when the initial prestress is 1350 Mpa. The unprestressed reinforcement ratio influences the bearing capacity of specimens more than the initial prestress.

(3) Mechanical properties of the beam-column interface when PPEFF nodes undergo the low-cyclic reciprocating loads are analyzed through experiments. The study finds that concrete strength grade, initial effective prestress of prestressed tendons, reinforcement ratio of prestressed

tendons, and reinforcement ratio of unprestressed tendons can influence the stress increment of prestressed tendons significantly. On this basis, the calculation formula of the stress increment is concluded. When the reduction coefficient is 0.28 under positive loading and 0.13 under negative loading, the calculated values of the formula agree well with the measured value in the test, indicating that the formula is reliable to a certain extent.

The PPEFF nodes in this study apply asymmetric hybrid joints. Under the premise of structural safety, they have good

mechanical properties, high construction efficiency, and low cost, thereby showing promising application potential. However, this study doesn't involve many specimens and thus obtains limited mechanical property indexes. Further studies on other parameters are still needed.

This is an Open Access article distributed under the terms of the Creative Commons Attribution License.



References

- Guan, D., Jiang, C., Guo, Z., Ge, H., "Development and Seismic Behavior of Precast Concrete Beam-to-Column Connections". *Journal of Earthquake Engineering*, 22(1-2), 2018, pp.234-256.
- Lee, D. J., Lee, J. D., Oh, T. S., Kang Thomas, T. H. K., "Seismic Experiment of Precast Concrete Exterior Beam-Column Joint Using Bolt Type Connection and Prestressing Method". *Journal of the Korea Concrete Institute*, 26(2), 2014, pp.125-133.
- Liang, P. X., Guo, Z. X., "Study on the performance hybrid connection interface of the beam and column". *Building Structure*, 41(10), 2011, pp.84-88.
- Said, S.H., Razak, H.A., "Structural behavior of RC engineered cementitious composite (ECC) exterior beam-column joints under reversed cyclic loading". *Construction And Building Materials*, 107, 2016, pp.226-234.
- Ghomi, S., El-Salakawy, E. F., "Effect of geometrical configuration on seismic behavior of GFRP-RC beam-column joints". *Advances in Concrete Construction*, 9(3), 2020, pp.313-326.
- Ali, A. M., Masmoudi, R., "Experimental and analytical investigation of new concrete filled FRP tube beam-column connections". *Engineering Structures*, 191, 2019, pp. 311-322.
- Khaloo, A., Bakhtiari Doost, R., "Seismic performance of precast RC column to steel beam connections with variable joint configurations". *Engineering Structures*, 168, 2018, pp. 408-418.
- Al-Osta, M. A., Al-Khatib, A. M., Baluch, M. H., Azad, A. K., Rahman, M. K., "Performance of hybrid beam-column joint cast with high strength concrete". *Earthquakes And Structures*, 12(6), 2017, pp. 603-617.
- Azimi, M., Bagherpourhamedani, A., Tahir, M. M., Sam, A. R. B. M., "Evaluation of new spiral shear reinforcement pattern for reinforced concrete joints subjected to cyclic loading". *Advances In Structural Engineering*, 19(5), 2016, pp. 730-745.
- Nzabonimpa, J. D., Hong, W. K., Park, S. C., "Experimental investigation of dry mechanical beam-column joints for precast concrete based frames". *Structural Design Of Tall And Special Buildings*, 26(1), 2017.
- Vidjeapriya, R., Jaya, K. P., "Experimental Study on Two Simple Mechanical Precast Beam-Column Connections under Reverse Cyclic Loading". *Journal of Performance of Constructed Facilities*, 27(4), 2013, pp. 402-414.
- Naik, C. B., Joshi, D. D., Patel, P.V., "Experimental Evaluation of Performance of Dry Precast Beam Column Connection". *Advances in Structural Engineering*, 2015, pp. 2333-2342.
- Aydin, A., Kilic, M., Maali, M., Sagioglu, M., "Experimental assessment of the semi-rigid connections behavior with angles and stiffeners". *Journal of Constructional Steel Research*, 114, 2015, pp. 338-348.
- Girgin, S. C., Misir, I.S., Kahraman, S., "Experimental Cyclic Behavior of Precast Hybrid Beam-Column Connections with Welded Components". *International Journal of Concrete Structures And Materials*, 11(2), 2017, pp. 229-245.
- Morgen, B.G., Kurama, Y.C., "A Friction Damper for Post-Tensioned Precast Concrete Moment Frames". *Prestressed Concrete Institute Journal*, 49(4), 2004, pp. 112-133.
- Morgen, B.G., Kurama, Y.C., "Seismic Design of Friction-Damped Precast Concrete Frame Structures". *Journal of Structural Engineering*, 133(11), 2007, pp. 1501-1511.
- Morgen, B. G., Kurama, Y. C., "Seismic response evaluation of post-tensioned precast concrete frames with friction dampers". In: 8th U.S. *National Conference on Earthquake Engineering*. 134(1), 2006, pp. 132-145.
- Zhang, C., Zhou, Y. L., Cai, X. N., Meng, S. P., "Experimental study on seismic behaviors of unbonded post-tensioned hybrid precast concrete frame joints". *Journal of Southeast University*, 46(05), 2016, pp. 1063-1069.
- Pan, P., Wang, H. S., Guo, H. S., Liu, K., Wang, D. Y., Qi, H., Geng, J., "Experimental study of seismic performance of unbonded post-tensioned pre-stressed beam-to-column dry connections". *Journal of Building Structures*, 39(10), 2018, pp. 46-55.
- Ministry of housing and urban-rural development, PRC., "Code for design of concrete structures". 2011.
- Wang, D. Y., Li, Z. B., Hang, Y., Hu, F.Q., "Seismic performance of post-tension tendons in pre-stressed assembly structures". *Journal of Building Structures*, 31(S1), 2010, pp. 333-338.